Complete classification of band nodal structures and massless excitations

Feng Tang* and Xiangang Wan†

National Laboratory of Solid State Microstructures and School of Physics, Nanjing University, Nanjing 210093, China and Collaborative Innovation Center of Advanced Microstructures, Nanjing University, Nanjing 210093, China

(Received 24 January 2022; accepted 21 April 2022; published 28 April 2022; corrected 2 June 2022)

Energy band nodal structures (nodal points/lines/surfaces) in the Brillouin zone (BZ) have received immense research interest in the past decade, while their complete classification is still lacking. Here, we focus on all the 1651 magnetic space groups (MSGs) and 528 magnetic layer groups (MLGs) to provide a dataset of all symmetry-diagonalizable strictly and nearly nodal structures emanating from band nodes (BNs) at symmetric k points. Using our dataset, one can quickly know their $k \cdot p$ models. Based on the $k \cdot p$ models, we find that charge-4 Weyl nodal point, thought to only exist in the spinless setting before, can exist in the spinful setting. Our dataset can also be applied to quickly identify the associated nodal structures, which can be composed of several nodal lines or/and surfaces given a BN. In this way, we identify nodal lines which are flexible but only fixed at one point in the BZ. Our classification includes both spinful and spinless settings with the latter applicable for bosons like phonons and electronic materials with negligible spin-orbit coupling. We show that the same as BNs, the nodal structures, especially the nearly nodal surfaces, are also ubiquitous. Finally, we predict hundreds of ever-synthesized magnetic materials with essential extended nodal lines or surfaces and one charge-4 Weyl magnetic material.

DOI: 10.1103/PhysRevB.105.155156

I. INTRODUCTION

The nodal structures in energy bands, classified by degeneracy, dimensionality (point, line or surface), topological charge etc., have attracted extensive attention [1–3] since they can underlie fascinating physical properties, like surface Fermi arcs [4], chiral anomaly [5], drumhead surface states [6], Klein tunneling [7], and so on. Most nodal structures can be deduced from isolated band nodes (BN) at symmetric k points while previously only specific aspects of the BN were focused on, for example, the location of the BN is at a high-symmetry point [8–14], the degeneracy is larger than 2 [8,9,11,12,14], and the low-energy dispersion should be linear [10,11], etc. Very recently, considering all BNs in high-symmetry points, high-symmetry lines and high-symmetry planes in the 230 space groups (SGs) with additional time-reversal (T) symmetry, Ref. [15] constructed a very useful encyclopedia by $k \cdot p$ modeling. They find that all possible degeneracies of BNs in crystals are 2, 3, 4, 6, and 8 and the largest topological charge is 4 [15]. Furthermore, it is found that when T symmetry is preserved, the charge-4 Weyl point (WP) only exists in the spinless setting [15,16], thus dubbed as spinless charge-4 WP here. However, when magnetic order is formed, there are another 1421 magnetic SGs (MSGs) describing magnetic three-dimensional (3D) systems [17], thus new types of massless excitations are anticipated. Besides, the 528 magnetic layer groups (MLGs) are also interesting for they describe symmetries of two-dimensional (2D) magnetic or nonmagnetic materials like graphene [18], as well as the boundaries between different insulating phases [19]. Then a complete classification of BNs in all 1651 MSGs and 528 MLGs is still lacking.

On the other hand, while the BNs have been well-investigated and predicted in specific conditions [8–10,13–15,20–28], the nodal structures have not. Though the nodal structures can be deduced by constructing $k \cdot p$ model around a BN [2,3,8,9,15,29], it can only predict local nodal structures around the BN. Moreover, the $k \cdot p$ model is commonly only expanded to a fixed order in $\mathbf{q}$ (the momentum measured from the BN) [2,3,8,9,15,29], thus whether including symmetry-allowed higher $k \cdot p$ terms could gap the predicted nodal structures is not yet known. Notably, the same as the strictly nodal structures, the nearly nodal structures could also bring about novel properties, such as the PT (P: inversion) protected nodal lines [6,30–32] and Dirac point in graphene when spin-orbit coupling (SOC) is neglected. All in all, a complete list of all possible BNs and both strictly and nearly nodal structures in the 1651 MSGs and 528 MLGs and in both spinful and spinless settings is not only important in revealing new types of BNs and nodal structures, and it is also useful for efficient materials predictions.

In this paper, we combine compatibility relations (CRs) and $k \cdot p$ models to obtain such a complete list: CRs can predict extended nodal structures, like nodal line along some high-symmetry line/within some high-symmetry plane and nodal surface along some high-symmetry plane since CRs tell us how bands split away from a BN. For reader's convenience, we summarize ten different CR-required band splitting patterns as shown in Table S1 in Supplemental Material [51] (including P-NP, P-NL, P-NS, P-NSL, L-NL, L-NP, L-sNL, L-NS, PL-NS, and PL-NL) so that one can know the dimensionality of nodal structure easily, for example, for CR-required band splitting pattern named by P-NSL, the nodal

*fengtang@nju.edu.cn
†xgwan@nju.edu.cn

TABLE I. Interpretations of ten CR-required band splitting patterns. Note that there might exist several nodal lines or nodal surfaces for P-NL, P-NS, and P-NSL, and they all coincide with high-symmetry line or plane. For L-NL, the nodal line(s) lie in high-symmetry plane(s), and multiple nodal lines constitute a nodal-chain structure. For L-sNL, the nodal line coincides with the high-symmetry line where the BN occurs. For P-NP, P-NL, P-NS, P-NSL, L-sNL, L-NS, and PL-NS, there is only one (co-)irrep in the BN while for the rest CR-required band splitting patterns, there are two different (co-)irreps.

Name of CR-required band splitting pattern	P-NP	P-NL
Meaning	The BN occurs at high-symmetry point, and is a nodal point	The BN occurs at high-symmetry point, lying in nodal line(s)
Name of CR-required band splitting pattern	P-NS	P-NSL
Meaning	The BN occurs at high-symmetry point, lying in nodal surface(s)	The BN occurs at high-symmetry point, lying in nodal line(s) and surface(s) simultaneously
Name of CR-required band splitting pattern	L-NP	L-NL
Meaning	The BN occurs in high-symmetry line, and is a nodal point	The BN occurs in high-symmetry line, lying in nodal line(s)
Name of CR-required band splitting pattern	L-sNL	L-NS
Meaning	The BN occurs in high-symmetry line, lying in a nodal line	The BN occurs in high-symmetry line, lying in nodal surface(s)
Name of CR-required band splitting pattern	PL-NL	PL-NS
Meaning	The BN occurs in high-symmetry plane, lying in a nodal line	The BN occurs in high-symmetry plane, lying in a nodal surface

structures of a BN at high-symmetry point contains coexisting nodal lines and surfaces (the reader can also find in Table I of the main text more detailed interpretations of the other CR-required splitting patterns). More details on classification can also be found in Supplemental Material [51]. It is worth mentioning that the extended nodal structures by CRs have a great chance of crossing the Fermi surfaces, significant in designing devices with large exotic quantum responses [52]. And $k \cdot p$ model can predict nearly nodal structures, be used to calculate topological charge and even predict strictly nodal structures beyond those by CRs. Our comprehensive results are given in datasets I–IV [53] in both top-down and bottom-up forms: dataset I displays all $k \cdot p$ models (expressed by H_i and h_j for MSGs and MLGs, respectively) complete to describe all possible BNs; dataset II gives concrete realizations of BNs for each $k \cdot p$ model. One can know all possible nodal structures by CRs in dataset III, which can be reproduced by $k \cdot p$ models but note that $k \cdot p$ models might give more nearly nodal structures by varying the expansion orders. Dataset IV gives concrete realizations of BNs for a given CR-required band splitting pattern.

II. METHODOLOGY AND NEW TYPES OF MASSLESS EXCITATIONS

Noticing that any symmetry-protected nodal structure owns at least one point (namely, the BN mentioned above), we can exhaust all possible symmetry-diagonalizable nodal structures by systematically analyzing all BNs located at high-symmetry point/line/plane. Starting from any BN, whose participating irreducible representation(s) (irrep(s)) or co-irrep(s) can be known from its little group, we exploit CRs to obtain how bands split in the vicinity of the BN, namely, the CR-required band splitting pattern [17,54]. From the CR-required band splitting pattern, we obtain all nodal structures (definitely strictly) emanating from the BN. These nodal structures required by CRs always exist as long as the BN is formed and can be extended in the Brillouin zone (BZ) when they coincide with high symmetry lines/surfaces. In order to obtain all nearly nodal structures, we then construct $k \cdot p$ models around all the BNs. Based on the explicit $k \cdot p$ models, we find that the charge-4 WP, believed to only exist in the spinless setting [15,16], can also exist in the spinful setting in several MSGs as shown in Table II: $SrCuTe_2O_6$ [55] is found to be crystallized in MSG 213.63 and thus could host the spinful charge-4 WP. The first-principles calculated electronic band structure is shown in Fig. S8 of Supplemental Material [51] which shows coexisting charge-4 and spin-1 WP below the Fermi level.

TABLE II. MSGs allowing spinful charge-4 WP. For all MSGs here, the charge-4 WP is pinned at high-symmetry point $(\frac{1}{2}, \frac{1}{2}, \frac{1}{2})$. All 2D (co-)irreps for this high-symmetry point in these MSGs correspond to spinful charge-4 WPs. Other than spinful charge-4 WPs, this high-symmetry point can also host triply-degenerate spin-1 WP [8]. H_{1415} and H_{1508} are the $k \cdot p$ models which can be found in dataset I: $H_{1415} = [R_2(q_z^2 - q_x^2) + R_3(q_y^2 - q_x^2)]\sigma_x + \frac{R_3(q_x^2+q_y^2-2q_z^2)+R_2(2q_y^2-q_x^2-q_z^2)}{\sqrt{3}}\sigma_y + R_4 q_x q_y q_z \sigma_z$ and $H_{1508} = R_2(q_z^2 - \frac{q_x^2+q_y^2}{2})\sigma_x + \frac{\sqrt{3}R_2(q_y^2-q_z^2)}{2}\sigma_y + R_3 q_x q_y q_z \sigma_z$.

Type	IV	I	IV	I	IV
MSG	198.11	212.59	212.62	213.63	213.66
H_i	H_{1415}	H_{1508}	H_{1508}	H_{1508}	H_{1508}

By comparing the nodal structures by CRs (namely from CR-required band splitting pattern) and those by $k \cdot p$ models, we prove that there exists a cutoff $k \cdot p$ order for any BN. For most BNs, we can find a least order to which the $k \cdot p$ model can give exactly the same nodal structures as those by CR-required band splitting pattern and such order can be chosen to be the cutoff order. For the rest BNs, we can also find a least cutoff $k \cdot p$ order which can not only reproduce all the nodal structures predicted by CR-required band splitting pattern but also provide additional strictly nodal structures. These additional nodal structures are all nodal lines and are missed when simply using CRs though. In the spinless setting, they can only be pinned at the BN and the rest part can be movable freely in the BZ, not ever unveiled before. An important usage of $k \cdot p$ models is that the $k \cdot p$ models up to the cutoff orders facilitate us to explore all nearly nodal structures by lowering the $k \cdot p$ orders. We find that the maximal cutoff order is 6, thus to obtain strictly nodal structures, $k \cdot p$ model up to 6th order is sufficient. Also, the cutoff order quantitatively characterizes the order of magnitude of the gap opened in the nearly nodal structures by considering higher-order $k \cdot p$ terms. Among 98970 BNs in total in MSGs, around 22.4% can have nearly nodal structures. For example, strictly nodal surface can only occur in very restricted symmetry conditions [15]. In total, 10636 BNs are found to lie in strictly nodal surfaces for some nonsymmorphic MSGs. However, nearly nodal surfaces can occur for another 19520 BNs. Concretely, there are only 254 (486) MSGs allowing strictly nodal surface while there are 789 (1316) MSGs allowing nearly nodal surfaces, in the spinful (spinless) setting. Such enrichment on nodal structures is expected to be important from an experimentalist's perspective. The nearly nodal structure in some material near the Fermi level can induce large responses even though the material cannot allow strictly nodal structure. In the following, we demonstrate examples of strictly nodal lines missed by CRs and nearly nodal surface.

III. NODAL LINES NOT CAPTURED BY CRS

As stated above, we find that there are several exceptions for which there exist more additional strictly nodal lines by $k \cdot p$ models than those by CRs. The CR-required band splitting patterns for these exceptions are: P-NP, L-NP, and P-NL (see Tables S4–S9 of Supplemental Material [51] for concrete $k \cdot p$ models). The corresponding BNs can be found in dataset II given H_i in these tables. These nodal lines are found to be protected by PT/mirror/glide symmetry, through checking the little groups for the BNs for these $k \cdot p$ models. For CR-required band splitting pattern P-NP, when the BN owns a mirror/glide symmetry, we find that for all BNs corresponding to Tables S4 and S5 of Supplemental Material [51], the eigenvalues of the mirror/glide operation are inverse. Since the BN is pinned at a high-symmetry point, there is no reason that the BN lies in a nodal line within a high-symmetry plane invariant under the mirror/glide operation. However, we use the explicit $k \cdot p$ models to solve for the nodal structures and find that strictly nodal lines are formed. Similarly, for CR-required band splitting pattern P-NL in Tables S8 and S9 of Supplemental Material [51], there exist more strictly nodal lines than those by CR-required band splitting patterns, also protected by some mirror/glide symmetry. For Tables S6 and S7 of Supplemental Material [51], the CR-required band splitting pattern can be P-NP, L-NP or P-NL, there exist more strictly nodal lines protected by PT symmetry in the spinless setting: Examples are shown below using the $k \cdot p$ models H_{2026} and H_{2373}. Interestingly, such PT protected nodal lines are fascinating since the points in these nodal lines are all flexible in the BZ other than the one pinned at the BN (thus can be diagnosed efficiently).

We first give an example of a BN formed by the crossing of two bands with two different co-irreps: single-valued co-irreps {1} and {3} [33], within high-symmetry line Λ or V of MSG 83.44 (type II). According to dataset III, the CR-required band splitting pattern is L-NP and the $k \cdot p$ model is H_{2026}. From dataset I, the $k \cdot p$ model H_{2026} is $[R_4(q_y^2 - q_x^2) + R_5 q_x q_y]\sigma_x + [R_6 q_z + R_7 q_z^2 + R_8(q_x^2 + q_y^2)]\sigma_z$ to the cutoff order 2 ($R_1, R_2, \ldots$ are all real parameters). Though CRs require that the $k \cdot p$ model H_{2026} should describe a nodal point by CR-required band splitting pattern L-NP, H_{2026} allows nodal line solutions, which are then found to be protected by PT symmetry. Figure 1(a) demonstrates the PT protected nodal lines where the concrete parameters are also given.

We then show another example, a BN formed at high-symmetry point Γ of MSGs 147.14, 147.16, 148.18, or 148.20, with a single-valued co-irrep being {2,6}. According to dataset III, its CR-required band splitting patten is P-NL, as shown in Fig. S3(a) of Supplemental Material [51], where the nodal structure can be found along the high-symmetry line Δ. The $k \cdot p$ model is $H_{2373} = [R_4(q_y^2 - q_x^2) + R_5 q_x q_z + R_3 q_y q_z + R_6 q_x q_y]\sigma_x + (-R_3 q_z q_x + 2R_4 q_x q_y + R_5 q_y q_z + R_6 \frac{q_x^2 - q_y^2}{2})\sigma_y$, from dataset I. Obviously, $q_x = 0$, $q_y = 0$ is the node solution of this model, namely, the corresponding nodal line is along z direction (parallel to the high-symmetry line Δ). However, there exist another three solutions corresponding to three nodal lines protected by PT symmetry, as demonstrated in Fig. 1(b) where we take all the parameters to be unity.

IV. $k \cdot p$ ORDER ENRICHED NODAL STRUCTURES

Then we show an example of BN whose cutoff order of $k \cdot p$ model is 6 to show nearly nodal structures by lowering $k \cdot p$ order. The BN is formed by two single-valued irreps 3 and 4 in the high-symmetry line Δ of MSG 183.185. As shown in Fig. S5(c) of Supplemental Material [51], the CR-required band splitting pattern for this BN is L-NL, namely, no matter how large the $k \cdot p$ order is, the CRs require that there should exist nodal lines [red lines in Fig. 1(c)] lying in high-symmetry planes [six gray planes in Fig. 1(c)] for this BN. The $k \cdot p$ model is H_{2469}, which is also a 2×2 matrix, whose explicit expression can be found in dataset I. As the cutoff order for this BN is 6, thus H_{2469} has the order of 6 in $\mathbf{q}$. As shown in Fig. 1(c), the yellow surface represents the node solution for the $k \cdot p$ model with order 2, while the cyan surface represents the node solution of the $k \cdot p$ model with order 1. The yellow curved surface in Fig. 1(c) is nearly but an almost strictly nodal surface, while the strictly nodal surface stabilized by MSG symmetries can only coincide with a high-symmetry plane [15]. In total, there are 796 out of the

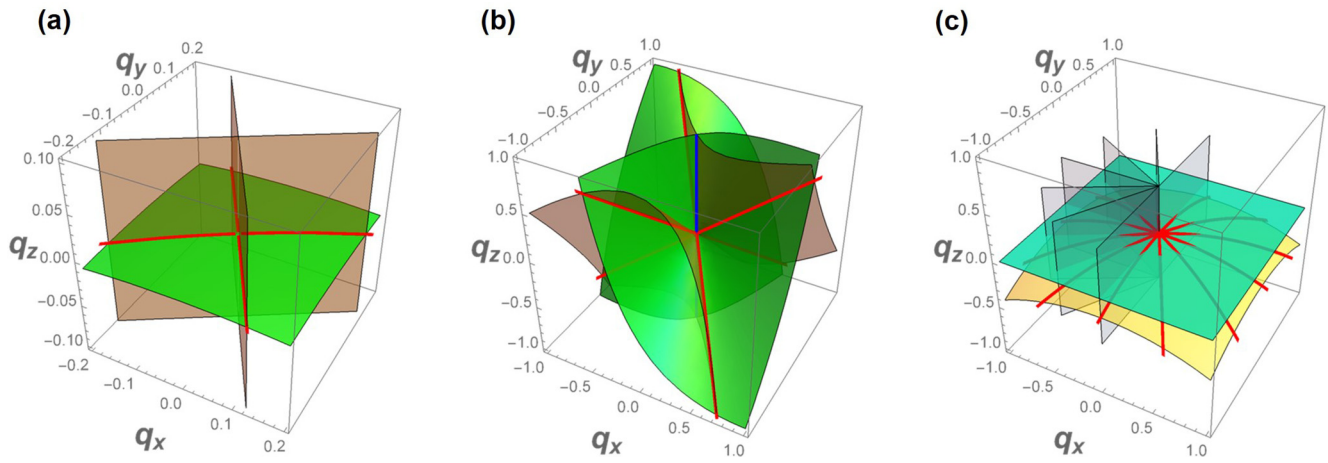

FIG. 1. *PT* protected nodal lines in (a) and (b), $k \cdot p$ order enriched nodal structures in (c). In (a), for the $k \cdot p$ model $H_{2026} = [R_4(q_y^2 - q_x^2) + R_5 q_x q_y]\sigma_x + [R_6 q_z + R_7 q_z^2 + R_8(q_x^2 + q_y^2)]\sigma_z$, whose CR-required band splitting pattern can only be L-NP, we choose the parameters $R_4 = R_5 = 0.1R_6 = R_7 = R_8 = 0.1$. The nodal lines for this $k \cdot p$ model can be visualized the intersection of two energy surfaces. The orange surface is $0.1(q_y^2 - q_x^2) + 0.1 q_x q_y = 0$ while the green surface is $(q_z + 0.1 q_z^2) + 0.1(q_x^2 + q_y^2) = 0$ and their intersection contains two nodal lines (in red) which are pinned at the BN located at the origin. In (b), for the $k \cdot p$ model $H_{2373} = [R_4(q_y^2 - q_x^2) + R_5 q_x q_z + R_3 q_y q_z + R_6 q_x q_y]\sigma_x + (-R_3 q_z q_x + 2R_4 q_x q_y + R_5 q_y q_z + R_6 \frac{q_x^2 - q_y^2}{2})\sigma_y$, whose CR-required band splitting pattern can be P-NL, we choose all the parameters to be 1. The orange surface is $q_y^2 - q_x^2 + q_x q_z + q_y q_z + q_x q_y = 0$ while the green surface is $-q_z q_x + 2q_x q_y + q_y q_z + \frac{q_x^2 - q_y^2}{2} = 0$. Their intersection contains one nodal line (in blue) along the q_z axis which is required by CR-required band splitting pattern and the other three nodal lines (in red) not required by CR-required band splitting pattern. (c) demonstrates the $k \cdot p$ order enriched nodal structures using the $k \cdot p$ model H_{2469}: The six nodal lines in red, lying in six high-symmetry planes (in gray) are required by CR-required band splitting pattern (the CR-required band splitting pattern is L-NL) but they only appear when the $k \cdot p$ order is 6 or larger. The cyan plane is along q_x-q_y plane which is the solution for nodes when the $k \cdot p$ order takes 1. The yellow surface is the solution for nodes when the $k \cdot p$ order is 2. When the $k \cdot p$ order is 3, 4, or 5, the yellow surface is almost still the node solution. The parameters we choose for the demonstration are shown in Sec. S8 of Supplemental Material [51].

3026 $k \cdot p$ models H_i's for MSGs found to show nearly nodal structures, corresponding to 22 159 BNs in total, which means that nearly $\frac{1}{4}$ of BNs can demonstrate $k \cdot p$ order enriched nodal structures. Concretely, among 98 970 BNs in total for all MSGs, we combine CRs and $k \cdot p$ models to reveal that 10636 can lie in strictly nodal surface (the CR-required band splitting pattern is P-NS, P-NSL, P-NSL, or PL-NS) and 60 200 can lie in strictly nodal lines (the CR-required band splitting pattern is P-NL, P-NSL, L-NL, L-sNL, or PL-NL), while 19 520 can lie in nearly nodal surface (the CR-required band splitting pattern is not P-NS, P-NSL, P-NSL, or PL-NS) and 57 can lie in nearly nodal lines (CR-required band splitting pattern is not P-NL, P-NSL, L-NL, L-sNL, or PL-NL). We list all MSGs realizing strictly or/and nearly nodal surfaces in spinless or/and spinful setting in Sec. S10 of Supplemental Material [51]. Overall, majority of MSGs allow nodal surfaces, while only nonsymmorphic MSGs can allow the formation of strictly nodal surface.

V. MATERIALS SEARCH

Finally we apply our results in the search for magnetic topological semimetals. Compared with the great advancements in the nonmagnetic topological materials [56,57], the field of topological magnetic materials [58] is still in its infancy possibly due to the scarcity of realistic magnetic materials with experimentally identified magnetic structures. Another intrinsic difficulty in predicting magnetic topological materials is originated in the electronic correlation, which should be treated very carefully in the first-principles calculations. Here we obtain a complete list of MSGs with essentially nodal surfaces and nodal lines, corresponding to the CR-required band splitting pattern PL-NS and L-sNL, respectively, as listed in detail in dataset V. The information on essentially nodal lines/surfaces in dataset V are thus useful for materials predictions, for both nonmagnetic and magnetic materials, and also applicable for bosonic excitations.

To date, the Bilbao MAGNDATA database [55] has collected more than 1500 magnetic materials. Here, simply by matching MSGs of the magnetic materials with the MSGs in the spinful setting shown in dataset V, we find hundreds of magnetic materials with commensurate magnetic structures listed in dataset V. In Table III of the main text, we list the stoichiometric magnetic materials whose chemical formulas exclude O and haloid elements. The present materials predictions are purely from symmetry and expected to be robust against weak electronic correlation [23,59–61], thus they are promising to be verified by experiments. Note that that these nodal lines/surfaces can be judged by the information at high-symmetry points according to the CR-required band splitting patterns P-NL, P-NS, P-NSL, all possible patterns of them being schematically shown in Fig. S7 of Supplemental Material [51]. Interestingly, for P-NL, the maximal number of the extended nodal lines emanating from the high-symmetry point, is found to be 13. We expect this exotic nodal structures, diagnosed simply using the symmetry information at high-symmetry point, could show fascinating quantum responses when electrons shuttle around these nodal lines.

TABLE III. Magnetic materials realizing charge-4 WP, symmetry-enforced essential and extended nodal line and surface. The materials are given by the entry label in Bilbao MAGNDATA database [55] and the chemical formula. The red/black/blue colors are for materials with charge-4 WP/essential nodal line/essential nodal surface, respectively, while the cyan color is for materials with coexisting essential nodal line and nodal surface.

1.136 : $AgCrS_2$	1.120 : $BaFe_2Se_3$	0.449 : Tb_2Pt	0.481 : HoNi	0.664 : Mn_3Sn_2	0.176 : $Mn_3Ti_2Te_6$	0.226 : $NiCo_2$	0.397 : $Mn_3Si_2Te_6$
0.690 : NdPt	2.10 : HoP	2.70 : GdMg	1.349 : $CoNb_3S_6$	0.710 : $MnNb_3S_6$	1.98 : $DyFe_4Ge_2$	1.335 : Nd_2Pd_2In	1.0.48 : $MnSe_2$
1.18 : MnS_2	2.51 : $EuMnBi_2$	0.768 : $SrMnSb_2$	1.444 : Er_2Pt	1.86 : GeV_4S_8	1.33 : ErAuGe	1.34 : HoAuGe	1.504 : GdCuSn
1.505 : GdAgSn	1.506 : GdAuSn	1.267 : $Dy_2Co_3Al_9$	1.67 : TmPtIn	0.342 : Tb_3Ge_5	0.345 : Tb_2C_3	1.632 : $ErFe_6Ge_6$	1.633 : YFe_6Sn_6
2.12 : TbMg	2.11 : TbMg	1.356 : Ho_3Ge_4	1.628 : $PrMnSi_2$	1.634 : YFe_6Ge_6	1.457 : $NdNiMg_{15}$	2.30 : $CeRh_2Si_2$	1.22 : DyB_4
0.468 : ErB_4	1.368 : $Tb_2Ni_3Si_5$	2.68 : $FeGe_2$	0.563 : $Ce_2Ni_3Ge_5$	1.362 : Er_3Ge_4	1.8 : $CeRu_2Al_{10}$	2.80 : $ErFe_6Ge_6$	2.57 : $TbMn_2Si_2$
2.60 : $NbMn_2Si_2$	1.252 : $CaCo_2P_2$	1.305 : Mn_5Si_3	1.460 : PrCuSi	2.67 : $FeSn_2$	0.562 : $Ce_2Ni_3Ge_5$	1.450 : $Pr_6Fe_{13}Sn$	1.556 : $FeSn_2$
1.557 : $FeGe_2$	2.31 : Mn_3ZnN	1.0.47 : $MnSe_2$	2.1 : $EuFe_2As_2$	0.185 : Nd_5Ge_4	0.408 : PrSi	0.437 : Ho_3NiGe_2	0.438 : Pr_3CoGe_2
0.480 : HoNi	0.685 : ErPt	0.686 : HoPt	0.688 : TmPt	0.407 : NdSi	0.409 : TmNi	0.445 : MnCoGe	0.684 : TbPt
0.687 : DyPt	0.439 : Tb_3NiGe_2	0.662 : Mn_3Sn_2	0.767 : $SrMnSb_2$	1.130 : Cr_2As	1.131 : Fe_2As	1.132 : Mn_2As	1.28 : CrN
1.507 : $NdPd_5Al_2$	2.36 : $TbGe_3$	1.334 : Pr_2Pd_2In	1.475 : $DyNiAl_4$	1.401 : Nd_5Pb_3	0.199 : Mn_3Sn	0.279 : Mn_3As	0.709 : $MnNb_4S_8$
0.711 : $MnTa_4S_8$	0.200 : Mn_3Sn	0.280 : Mn_3As	0.377 : Mn_3Ge	0.706 : $Tb_2Ir_3Ga_9$	0.771 : $PrMnSi_2$	0.774 : $NdMnSi_2$	0.776 : $CeMnSi_2$
0.778 : $LaMnSi_2$	3.3 : Ho_2RhIn_8	0.149 : $Nd_3Ru_4Al_{12}$	0.173 : $Pr_3Ru_4Al_{12}$	0.395 : MnPtGa	0.561 : $NdNiGe_2$	0.689 : PrPt	1.195 : Er_2Ni_2In
1.415 : Tb_2Pd_2In	1.446 : $CeCoAl_4$	3.13 : CeB_6	1.392 : $KCuMnS_2$	1.142 : CeMgPb	0.403 : $NdCo_2$	2.28 : $NpNiGa_5$	0.184 : Nd_5Si_4
1.85 : $\alpha - Mn$	1.152 : Ce_3NIn	1.574 : NdBiPt	0.448 : Ce_4Ge_3	0.681 : Ce_4Sb_3	2.44 : $KCuMnS_2$	1.451 : $Nd_6Fe_{13}Sn$	2.14 : NdMg
1.253 : $CeCo_2P_2$	1.425 : UGeTe	1.453 : $EuMn_2Si_2$	1.468 : $TbMn_2Si_2$	1.469 : YMn_2Si_2	1.488 : $CeMn_2Si_2$	1.491 : $PrMn_2Si_2$	1.493 : $NdMn_2Si_2$
1.496 : YMn_2Ge_2	0.320 : U_2Pd_2In	0.321 : U_2Pd_2Sn	1.102 : U_2Ni_2In	0.593 : UPSe	0.594 : UAsS	1.215 : UP_2	1.271 : CeSbTe
1.384 : USb_2	1.426*U GeS*	1.535 UPd_2Ge_2	1.143 : Mn_3Pt	2.13 : UP	2.20 : UAs	1.103 : U_2Rh_2Sn	1.479 : U_2Ni_2Sn
1.539 : KMnP	1.541 : RbMnP	1.543 : RbMnAs	1.545 : RbMnBi	1.546 : CsMnBi	1.547 : CsMnP	1.550 : LiMnAs	1.553 : KMnAs
0.236 : $CaFe_4Al_8$	0.324 : $CdYb_2S_4$	0.325 : $CdYb_2Se_4$	0.227 : $NdCo_2$	0.613 : $FeCr_2S_4$	0.169 : U_3As_4	0.170 : U_3P_4	2.32 : $Dy_3Ru_4Al_{12}$
0.286 : Mn_5Ge_3	0.673 : $MnFe_4Si_3$	0.528 : CrSb	1.412 : $Au_{72}Al_{14}Tb_{14}$	0.150 : NiS_2	0.20 : $MnTe_2$	3.6 : DyCu	0.440 : $SrCuTe_2O_6$

VI. CONCLUSIONS

To conclude, we obtained a comprehensive classification of all BNs and their nodal structures in all the 1651 MSGs and 528 MLGs for both spinful and spinless settings. Notably, considering nearly nodal structures leads to more fruitful band nodal structures. The new types of massless excitations: charge-4 spinful WP, Weyl nodal lines pinned at high-symmetry points/lines and $k \cdot p$ order enriched curved nodal surface can be realized in concrete materials. The magnetic materials shown in Table III for extended nodal lines/surfaces are expected to be verified experimentally in near future.

Note added. During the review of the work, we are aware of two related works [62,63], which classify band nodes by $k \cdot p$ models in type-III and type-IV magnetic space groups.

ACKNOWLEDGMENTS

F.T. was supported by National Natural Science Foundation of China (NSFC) under Grants No. 12104215. F.T. and X.W. were supported by the National Key R&D Program of China (Grants No. 2018YFA0305704), NSFC Grants No. 12188101, 11834006, 51721001, and 11790311, and the excellent program at Nanjing University. X.W. also acknowledges the support from the Tencent Foundation through the XPLORER PRIZE.

[1] T. O. Wehling, A. M. Black-Schaffer, and A. V. Balatsky, Dirac materials, Adv. Phys. **63**, 1 (2014).
[2] N. P. Armitage, E. J. Mele, and A. Vishwanath, Weyl and Dirac semimetals in three-dimensional solids, Rev. Mod. Phys. **90**, 015001 (2018).
[3] B. Q. Lv, T. Qian, and H. Ding, Experimental perspective on three-dimensional topological semimetals, Rev. Mod. Phys. **93**, 025002 (2021).
[4] X. Wan, A. M. Turner, A. Vishwanath, and S. Y. Savrasov, Topological semimetal and Fermi-arc surface states in the electronic structure of pyrochlore iridates, Phys. Rev. B **83**, 205101 (2011).
[5] D. T. Son and B. Z. Spivak, Chiral anomaly and classical negative magnetoresistance of Weyl metals, Phys. Rev. B **88**, 104412 (2013).
[6] A. A. Burkov, M. D. Hook, and L. Balents, Topological nodal semimetals, Phys. Rev. B **84**, 235126 (2011).
[7] M. I. Katsnelson, K. S. Novoselov, and A. K. Geim, Chiral tunneling and the Klein Paradox in Graphene, Nat. Phys. **2**, 620 (2006).
[8] B. Bradlyn, J. Cano, Z. Wang, M. G. Vergniory, C. Felser, R. J. Cava, and B. A. Bernevig, Beyond Dirac and Weyl fermions: Unconventional quasiparticles in conventional crystals, Science **353**, aaf5037 (2016).
[9] J. Cano, B. Bradlyn, and M. G. Vergniory, Multifold nodal points in magnetic materials, APL Mater. **7**, 101125 (2019).
[10] J. L. Mañes, Existence of bulk chiral fermions and crystal symmetry, Phys. Rev. B **85**, 155118 (2012).
[11] S. M. Young, S. Zaheer, J. C. Y. Teo, C. L. Kane, E. J. Mele, and A. M. Rappe, Dirac Semimetal in Three Dimensions, Phys. Rev. Lett. **108**, 140405 (2012).
[12] B. J. Wieder, Y. Kim, A. M. Rappe, and C. L. Kane, Double Dirac Semimetals in Three Dimensions, Phys. Rev. Lett. **116**, 186402 (2016).
[13] G. C. *et al.*, Topological quantum properties of chiral crystals, Nat. Mater. **17**, 978 (2018).
[14] B.-J. Yang and N. Nagaosa, Classification of stable three-dimensional Dirac semimetals with nontrivial topology, Nat. Commun. **5**, 4898 (2014).
[15] Z.-M. Yu, Z. Zhang, G.-B. Liu, W. Wu, X.-P. Li, R.-W. Zhang, S. A. Yang, and Y. Yao, Encyclopedia of emergent particles in three-dimensional crystals, Sci. Bull. **67**, 375 (2022).
[16] T. Zhang, R. Takahashi, C. Fang, and S. Murakami, Twofold quadruple Weyl nodes in chiral cubic crystals, Phys. Rev. B **102**, 125148 (2020).
[17] C. J. Bradley and A. P. Cracknell, *The Mathematical Theory of Symmetry in Solids* (Oxford University Press, Oxford, 1972)
[18] K. S. Novoselov, A. K. Geim, S. V. Morozov, D. Jiang, Y. Zhang, S. V. Dubonos, I. V. Grigorieva, and A. A. Firsov, Electric field effect in atomically thin carbon film, Science **306**, 666 (2004).
[19] B. J. Wieder *et al.*, Wallpaper fermions and the nonsymmorphic Dirac insulator, Science **361**, 246 (2018).
[20] J. Kruthoff, J. de Boer, J. van Wezel, C. L. Kane, and R.-J. Slager, Topological Classification of Crystalline Insulators through Band Structure Combinatorics, Phys. Rev. X **7**, 041069 (2017).
[21] R.-J. Slager, A. Mesaros, V. Juričić, and J. Zaanen, The space group classification of topological band-insulators, Nat. Phys. **9**, 98 (2013).
[22] H. C. Po, A. Vishwanath, and H. Watanabe, Symmetry-based indicators of band topology in the 230 space groups, Nat. Commun. **8**, 50 (2017).
[23] H. Watanabe, H. C. Po, and A. Vishwanath, Structure and topology of band structures in the 1651 magnetic space groups, Sci. Adv. **4**, aat8685 (2018).
[24] T. Zhang, Y. Jiang, Z. Song, H. Huang, Y. He, Z. Fang, H. Weng, and C. Fang, Catalogue of topological elecronic materials, Nature (London) **566**, 475 (2019).
[25] M. G. Vergniory, L. Elcoro, C. Felser, N. Regnault, B. A. Bernevig, and Z. Wang, A complete catalogue of high-quality topological materials, Nature (London) **566**, 480 (2019).
[26] F. Tang, H. C. Po, A. Vishwanath, and X. Wan, Comprehensive search for topological materials using symmetry indicators, Nature (London) **566**, 486 (2019).
[27] Y. Xu, L. Elcoro, Z.-D. Song, B. J. Wieder, M. G. Vergniory, N. Regnault, Y. Chen, C. Felser, and B. A. Bernevig, High-throughput calculations of magnetic topological materials, Nature (London) **586**, 702 (2020).
[28] B. Bradlyn, L. Elcoro, J. Cano, M. G. Vergniory, Z. Wang, C. Felser, M. I. Aroyo, and B. A. Bernevig, Topological quantum chemistry, Nature (London) **547**, 298 (2017).

[29] J. Yang, C. Fang, and Z.-X. Liu, Symmetry-protected nodal points and nodal lines in magnetic materials, Phys. Rev. B **103**, 245141 (2021).
[30] C. Fang, Y. Chen, H.-Y. Kee, and L. Fu, Topological nodal line semimetals with and without spin-orbital coupling, Phys. Rev. B **92**, 081201(R) (2015).
[31] R. Yu, H. Weng, Z. Fang, X. Dai, and X. Hu, Topological Node-Line Semimetal and Dirac Semimetal State in Antiperovskite Cu_3PdN, Phys. Rev. Lett. **115**, 036807 (2015).
[32] Y. Kim, B. J. Wieder, C. L. Kane, and A. M. Rappe, Dirac Line Nodes in Inversion-Symmetric Crystals, Phys. Rev. Lett. **115**, 036806 (2015).
[33] F. Tang and X. Wan, Exhaustive construction of effective models in 1651 magnetic space groups, Phys. Rev. B **104**, 085137 (2021).
[34] Z. Wang, Y. Sun, X.-Q. Chen, C. Franchini, G. Xu, H. Weng, X. Dai, and Z. Fang, Dirac semimetal and topological phase transitions in A_3 Bi (A = Na, K, Rb), Phys. Rev. B **85**, 195320 (2012).
[35] Z. Wang, H. Weng, Q. Wu, X. Dai, and Z. Fang, Three-dimensional Dirac semimetal and quantum transport in Cd_3As_2, Phys. Rev. B **88**, 125427 (2013).
[36] N. V. Belov, N. N. Neronova, and T. S. Smirnova, Shubnikov groups, Sov. Phys. Crystallogr. **2**, 311 (1957).
[37] D. Xiao, M.-C. Chang, and Q. Niu, Berry phase effects on electronic properties, Rev. Mod. Phys. **82**, 1959 (2010).
[38] W. Wu, Y. Liu, S. Li, C. Zhong, Z. M. Yu, X. L. Sheng, Y. X. Zhao, and S. A. Yang, Nodal surface semimetals: Theory and material realization, Phys. Rev. B **97**, 115125 (2018).
[39] H. Weng, C. Fang, Z. Fang, B. A. Bernevig, and X. Dai, Weyl Semimetal Phase in Noncentrosymmetric Transition-Metal Monophosphides, Phys. Rev. X **5**, 011029 (2015).
[40] S.-M. Huang, C. Fang, Z. Fang, B. A. Bernevig, and X. Dai, A Weyl Fermion semimetal with surface Fermi arcs in the transition metal monopnictide TaAs class, Nat. Commun. **6**, 7373 (2015).
[41] W. Chen, H.-Z. Lu, and J.-M. Hou, Topological semimetals with a double-helix nodal link, Phys. Rev. B **96**, 041102(R) (2017).
[42] Z. Yan, R. Bi, H. Shen, L. Lu, S.-C. Zhang, and Z. Wang, Nodal-link semimetals, Phys. Rev. B **96**, 041103 (2017).
[43] M. Ezawa, Topological semimetals carrying arbitrary Hopf numbers: Fermi surface topologies of a Hopf link, Solomon's knot, trefoil knot, and other linked nodal varieties, Phys. Rev. B **96**, 041202(R) (2017).
[44] P.-Y. Chang and C.-H. Yee, Weyl-link semimetals, Phys. Rev. B **96**, 081114(R) (2017).
[45] R. Bi, Z. Yan, L. Lu, and Z. Wang, Nodal-knot semimetals, Phys. Rev. B **96**, 201305 (2017).
[46] G. Chang, S. Y. Xu, X. Zhou, S. M. Huang, B. Singh, B. Wang, I. Belopolski, J. Yin, S. Zhang, A. Bansil, H. Lin, and M. Z. Hasan, Topological Hopf and Chain Link Semimetal States and Their Application to co_2MnGa, Phys. Rev. Lett. **119**, 156401 (2017).
[47] Y. Zhou, F. Xiong, X. Wan, and J. An, Hopf-link topological nodal-loop semimetals, Phys. Rev. B **97**, 155140 (2018).
[48] M. Fruchart, Y. Zhou, and V. Vitelli, Dualities and non-abelian mechanics, Nature (London) **577**, 636 (2020).
[49] V. Közii, J. W. F. Venderbos, and L. Fu, Three-dimensional majorana fermions in chiral superconductors, Sci. Adv. **2**, e1601835 (2016).
[50] S. Ono and K. Shiozaki, Symmetry-Based Approach to Nodal Structures: Unification of Compatibility Relations and Gapless Point Classifications, Phys. Rev. X **12**, 011021 (2022).
[51] See Supplemental material at http://link.aps.org/supplemental/10.1103/PhysRevB.105.155156 for detailed descriptions of classification of BNs and nodal structures based on CR-required band splitting patterns, matrix basis for each $k \cdot p$ model and the BNs showing more nodal lines using $k \cdot p$ models than simply using CRs. See also Refs. [4,6,8,9,15,17,30,33–50] therein.
[52] M. A. Wilde *et al.*, Symmetry-enforced topological nodal planes at the Fermi surface of a chiral magnet, Nature (London) **594**, 374 (2021).
[53] All these dataset files can be downloaded in https://drive.google.com/file/d/1HiQ6orMDqTBZzKcgVqodg9AZ7D2AOn8C/view?usp=sharing.
[54] M. I. Aroyo, A. Kirov, C. Capillas, J. M. Perez-Mato, and H. Wondratschek, Bilbaocrystallographic server. II. Representations of crystallographic point groups and space groups, Acta Crystallogr. A **62**, 115 (2006).
[55] http://webbdcrista1.ehu.es/magndata/.
[56] A. Bansil, H. Lin, and T. Das, Colloquium: Topological band theory, Rev. Mod. Phys. **88**, 021004 (2016).
[57] É. Lantagne-Hurtubise and M. Franz, Topology in abundance, Nat. Rev. Phys. **1**, 183 (2019).
[58] Y. Tokura, K. Yasuda, and A. Tsukazaki, Magnetic topological insulators, Nat. Rev. Phys. **1**, 126 (2019).
[59] H. Watanabe, H. C. Po, M. P. Zaletel, and A. Vishwanath, Filling-Enforced Gaplessness in Band Structures of the 230 Space Groups, Phys. Rev. Lett. **117**, 096404 (2016).
[60] R. Chen, H. C. Po, J. B. Neaton, and A. Vishwanath, Topological materials discovery using electron filling constraints, Nat. Phys. **14**, 55 (2018).
[61] D. Wang, F. Tang, H. C. Po, A. Vishwanath, and X. Wan, XFe_4 Ge_2(X=Y, Lu) and Mn_3 Pt: Filling-enforced magnetic topological metals, Phys. Rev. B **101**, 115122 (2020).
[62] G.-B. Liu, Z. Zhang, Z.-M. Yu, S. A Yang, and Y. Yao, Systematic investigation of emergent particles in type-iii magnetic space groups, Phys. Rev. B **105**, 085117 (2022).
[63] Z. Zhang, G.-B. Liu, Z.-M. Yu, S. A Yang, and Y. Yao, Encyclopedia of emergent particles in type-iv magnetic space groups, Phys. Rev. B **105**, 104426 (2022).

Correction: The URL in Ref. [53] was incorrect and has been fixed.